Exact Quantum Many-Body Scar States in the Rydberg-Blockaded Atom Chain

Cheng-Ju Lin and Olexei I. Motrunich

Exact Quantum Many-body Scar States in the Rydberg-blockaded Atom Chain

Cheng-Ju Lin and Olexei I. Motrunich
Department of Physics and Institute for Quantum Information and Matter,
California Institute of Technology, Pasadena, CA 91125, USA
(Dated: January 14, 2019)

A recent experiment in the Rydberg atom chain observed unusual oscillatory quench dynamics with a charge density wave initial state, and theoretical works identified a set of many-body "scar states" showing nonthermal behavior in the Hamiltonian as potentially responsible for the atypical dynamics. In the same nonintegrable Hamiltonian, we discover several eigenstates at *infinite temperature* that can be represented exactly as matrix product states with *finite* bond dimension, for both periodic boundary conditions (two exact $E = 0$ states) and open boundary conditions (two $E = 0$ states and one each $E = \pm\sqrt{2}$). This discovery explicitly demonstrates violation of strong eigenstate thermalization hypothesis in this model and uncovers exact quantum many-body scar states. These states show signatures of translational symmetry breaking with period-2 bond-centered pattern, despite being in one dimension at infinite temperature. We show that the nearby many-body scar states can be well approximated as "quasiparticle excitations" on top of our exact $E = 0$ scar states, and propose a quasiparticle explanation of the strong oscillations observed in experiments.

Introduction.- Understanding quantum thermalization in isolated systems has attracted a lot of attention, both due to developments in cold atom experiments and fundamental theoretical interest. Eigenstate thermalization hypothesis (ETH) has emerged as a paradigmatic mechanism for quantum thermalization [1, 2]. ETH postulates that a generic many-body system thermalizes at the level of individual eigenstates: Eigenstates at the same energy density give the same expectation values of "local-enough" observables. The strong version of ETH requires this on *every* eigenstate. While an analytical proof is elusive, many numerical studies provided strong corroborations [3–6]. However, some systems showed atypical dynamics [7, 8] due to special low-energy states [9–11].

A recent Rydberg cold atom experiment [12] hinted a new scenario, where the system exhibited atypical quench dynamics starting from a charge density wave (CDW) state at effective temperature $T = \infty$. In contrast, a uniform initial state with the same energy density showed the expected thermalization behavior. References [13, 14] proposed that this phenomenon is related to the presence of special eigenstates—*quantum many-body scar states*—which violate ETH in the otherwise thermal spectrum, analogous to the nonergodic single-particle scar wavefunctions inside the chaotic single-particle spectrum [15].

Another nonintegrable system hosting nonthermal eigenstates is the Affleck-Lieb-Kennedy-Tasaki (AKLT) model [16]. Reference [17] constructed families of exact eigenstates in this model. Using matrix product states (MPS), further Ref. [18] showed that these exact eigenstates with finite energy density have logarithmic entanglement scaling in the subsystem size. These papers thus provided important analytical demonstration of exact scar states that violate ETH [19]. Other works [20, 21] also proposed a special construction to embed nonthermal eigenstates into the many-body spectrum.

Remarkably, in the same Rydberg atom Hamiltonian studied in Refs. [12–14, 22, 23], we have discovered some exact scar states with *finite bond dimension* at energy density corresponding to $T = \infty$. Our exact MPS description shows that these exact scar states have constant entanglement scaling and are hence even more "nonthermal" than the exact scar states at finite energy density in Refs. [17, 18]. Furthermore, these exact scar states break the lattice translation symmetry, despite being at $T = \infty$. Thus, the strong-ETH is violated in the Rydberg atom chain. Using "single-mode approximation" (SMA) and generizing it to "multi-mode approximation" (MMA) on top of our exact scar states, we also find good approximations to nearby scar states, potentially relating the existence of other scar states to our exact states.

Constrained Hilbert space and Hamiltonian.- Consider Rydberg atoms on a chain with L sites, and denote $|0\rangle$ as the atomic ground state and $|1\rangle$ as the Rydberg excitation. The Rydberg blockade prohibits states with $|\ldots 11 \ldots\rangle$ on any two neighboring sites [12]. Despite the resulting non–tensor-product structure of the Hilbert space, one can still have ETH concept [24].

The dynamics of this system is described by so-called PXP model:

$$H = \sum_{j=2}^{L-1} P_{j-1} X_j P_{j+1} + H_1 + H_L \ , \qquad (1)$$

where $P = |0\rangle\langle 0|$ is the projector to the Rydberg atom ground state and $X = |0\rangle\langle 1| + |1\rangle\langle 0|$ describes transitions between the ground and excited states. (Previous works [25–28] studied low-energy states of related Hamiltonians.) For periodic boundary conditions (PBC), we have $H_1 = P_L X_1 P_2$ and $H_L = P_{L-1} X_L P_1$; while for open boundary conditions (OBC), $H_1 = X_1 P_2$ and $H_L = P_{L-1} X_L$. For PBC, the Hamiltonian has translation symmetry T_x and inversion symmetry I; while for OBC, there is only inversion symmetry relative to the

midpoint, $I : j \to L-j+1$. Furthermore, one can define "particle-hole transformation" $\mathcal{C}_{\mathrm{ph}} = \prod_j Z_j$, where $Z = |1\rangle\langle 1| - |0\rangle\langle 0|$. This satisfies $\mathcal{C}_{\mathrm{ph}} H \mathcal{C}_{\mathrm{ph}}^{-1} = -H$, which guarantees that the spectrum is symmetric around zero energy; moreover, intertwining of $\mathcal{C}_{\mathrm{ph}}$ with the inversion symmetry produces exponentially many zero-energy eigenstates [14, 29].

The above Hamiltonian, despite its simple appearance, is not trivially solvable. While its level-spacing statistics indicates its nonintegrability [14], a recent work [23] has suggested that it could be a deformation from some integrable Hamiltonian.

Inspired by Ref. [17], we inspected entanglement spectra of eigenstates of the PXP model for OBC and discovered eigenstates at $E = \pm\sqrt{2}$ with finite bond dimension. We then reverse-engineered simple MPS representation for these eigenstates and further identified two more exact eigenstates with $E = 0$ for OBC and two exact eigenstates at $E = 0$ for PBC. Hence, these states analytically demonstrate that the PXP Hamiltonian violates strong-ETH and are therefore *exact* quantum many-body scar states.

Exact scar states for PBC.- These eigenstates exist for even L (assumed throughout) and are expressed using MPS. We define 2×3 and 3×2 matrices

$$B^0 = \begin{pmatrix} 1 & 0 & 0 \\ 0 & 1 & 0 \end{pmatrix}, \qquad B^1 = \sqrt{2}\begin{pmatrix} 0 & 0 & 0 \\ 1 & 0 & 1 \end{pmatrix}, \qquad (2)$$

$$C^0 = \begin{pmatrix} 0 & -1 \\ 1 & 0 \\ 0 & 0 \end{pmatrix}, \qquad C^1 = \sqrt{2}\begin{pmatrix} 1 & 0 \\ 0 & 0 \\ -1 & 0 \end{pmatrix}. \qquad (3)$$

Two (unnormalized) exact scar states for PBC can be expressed as

$$|\Phi_1\rangle = \sum_{\{\sigma\}} \mathrm{Tr}[B^{\sigma_1} C^{\sigma_2} \ldots B^{\sigma_{L-1}} C^{\sigma_L}]|\sigma_1 \ldots \sigma_L\rangle, \quad (4)$$

and $|\Phi_2\rangle = T_x|\Phi_1\rangle$, where $\sigma_j = 0$ or 1. The wavefunctions satisfy the constraints since $B^1 C^1 = 0_{2\times2}$ and $C^1 B^1 = 0_{3\times3}$. In Supplemental Material [30], we prove $H|\Phi_i\rangle = 0$. Since these states are at $E = 0$, their effective temperature is $T = \infty$.

The norm of the states are $\langle\Phi_i|\Phi_i\rangle = 3^{L_b} + 2 + (-1)^{L_b}$, where $L_b \equiv L/2$. The two states are not orthogonal and have overlap $\langle\Phi_1|\Phi_2\rangle = 2[(\sqrt{2}-1)^{L_b} + (-1)^{L_b}(\sqrt{2}+1)^{L_b}]$; however, they are linearly independent for $L_b > 3$ [for $L_b \leq 3$, we happen to have $|\Phi_2\rangle = (-1)^{L_b}|\Phi_1\rangle$]. For $L_b > 3$, the states $|\Phi_{1,2}\rangle$ in fact break the translation symmetry T_x, while by construction they are invariant under T_x^2. One can form degenerate states $|\Phi_{K=0/\pi}\rangle = |\Phi_1\rangle \pm |\Phi_2\rangle$ that carry definite momenta 0 and π, which can be viewed as a finite-size signature of the T_x breaking that appears in the thermodynamic limit.

Let us examine properties of the state $|\Phi_1\rangle$ (properties of $|\Phi_2\rangle$ simply follow). First, the breaking of T_x in this state cannot be detected by any one-site observable,

since the one-site reduced density matrices are the same for all sites, $\rho^{\mathrm{one\text{-}site}} = \frac{2}{3}|0\rangle\langle 0| + \frac{1}{3}|1\rangle\langle 1|$ in the thermodynamic limit [30]. In particular, for the Rydberg excitation number $n_j = |1\rangle\langle 1|$, we have $\langle\Phi_1|n_j|\Phi_1\rangle/\langle\Phi_1|\Phi_1\rangle = \frac{1}{3}$. This violates ETH, since at $T = \infty$, the Gibbs ensemble predicts $\langle n_j\rangle_{T=\infty} = (1 + \phi^2)^{-1} \approx 0.2764$, where $\phi = (1 + \sqrt{5})/2$ is the golden ratio.

On the other hand, two-site observables can detect the T_x breaking, as can be seen from the corresponding reduced density matrices for subsystems $[1, 2]$ and $[2, 3]$ in the $|\Phi_1\rangle$ state:

$$\rho^{\mathrm{two\text{-}site}}_{[1,2]} = \frac{1}{3}(|00\rangle\langle 00| + |01\rangle\langle 01| + |10\rangle\langle 10|), \quad (5)$$

$$\rho^{\mathrm{two\text{-}site}}_{[2,3]} = \frac{1}{3}(|00\rangle\langle 00| + |01\rangle\langle 01| + |10\rangle\langle 10|)$$
$$- \frac{1}{9}(|01\rangle\langle 10| + |10\rangle\langle 01|). \quad (6)$$

In particular, we see that $|0_j 1_{j+1}\rangle\langle 1_j 0_{j+1}| + \mathrm{H.c.}$ has expectation value 0 for j odd and $-2/9$ for j even.

We also list the symmetry properties of these exact scar states (see [30] for the proof). For L even, the inversion I defined earlier is relative to a bond center and is not broken. We find $I|\Phi_1\rangle = (-1)^{L_b}|\Phi_1\rangle$. For $|\Phi_2\rangle$, note that since $IT_x = T_x^{-1}I$ and $T_x^2|\Phi_i\rangle = |\Phi_i\rangle$, we obtain also $I|\Phi_2\rangle = (-1)^{L_b}|\Phi_2\rangle$. While $\mathcal{C}_{\mathrm{ph}}$ is not a symmetry of H, our states are in fact eigenstates of $\mathcal{C}_{\mathrm{ph}}$. We have $\mathcal{C}_{\mathrm{ph}}|\Phi_i\rangle = (-1)^{L_b}|\Phi_i\rangle$ for both $i = 1, 2$.

Exact scar states for OBC.- We also found exact scar states for OBC with the same bulk MPS. Defining "boundary vectors" $v_1 = (1, 1)^T$ and $v_2 = (1, -1)^T$, we can write four exact scar states

$$|\Gamma_{\alpha,\beta}\rangle = \sum_{\{\sigma\}} v_\alpha^T B^{\sigma_1} C^{\sigma_2} \ldots B^{\sigma_{L-1}} C^{\sigma_L} v_\beta |\sigma_1 \ldots \sigma_L\rangle, \quad (7)$$

where $\alpha, \beta \in \{1, 2\}$. The eigen-energies are $E = 0$ for $|\Gamma_{\alpha,\alpha}\rangle$, $E = \sqrt{2}$ for $|\Gamma_{1,2}\rangle$, and $E = -\sqrt{2}$ for $|\Gamma_{2,1}\rangle$, see [30].

It is interesting to examine the energy density profiles. Figure 1(a)(b) shows $\langle X_j\rangle_{\alpha,\beta} \equiv \langle\Gamma_{\alpha,\beta}|X_j|\Gamma_{\alpha,\beta}\rangle/\langle\Gamma_{\alpha,\beta}|\Gamma_{\alpha,\beta}\rangle$ in each state [30]. We can see that there are localized "energy lumps" at the edges of the chain. The profiles decay exponentially into the bulk with decay length $2\ln(3)$. The integrated energy over each lump is $\sqrt{2}/2$ or $-\sqrt{2}/2$ depending on the termination, which can be thought as representing different "edge states."

The symmetry properties of $|\Gamma_{\alpha,\beta}\rangle$ can be derived in a similar fashion as for PBC [30]. In particular, we have $I|\Gamma_{1,2}\rangle = (-1)^{L_b-1}|\Gamma_{1,2}\rangle$ and $I|\Gamma_{2,1}\rangle = (-1)^{L_b-1}|\Gamma_{2,1}\rangle$; while $I|\Gamma_{1,1}\rangle = (-1)^{L_b}|\Gamma_{2,2}\rangle$ and $I|\Gamma_{2,2}\rangle = (-1)^{L_b}|\Gamma_{1,1}\rangle$. As for the particle-hole transformation, we obtain $\mathcal{C}_{\mathrm{ph}}|\Gamma_{1,2}\rangle = (-1)^{L_b}|\Gamma_{2,1}\rangle$ and $\mathcal{C}_{\mathrm{ph}}|\Gamma_{1,1}\rangle = (-1)^{L_b}|\Gamma_{2,2}\rangle$. The fact that $|\Gamma_{1,2}\rangle$ and $|\Gamma_{2,1}\rangle$ are eigenstates of I means that they can be nondegenerate, which is what we found
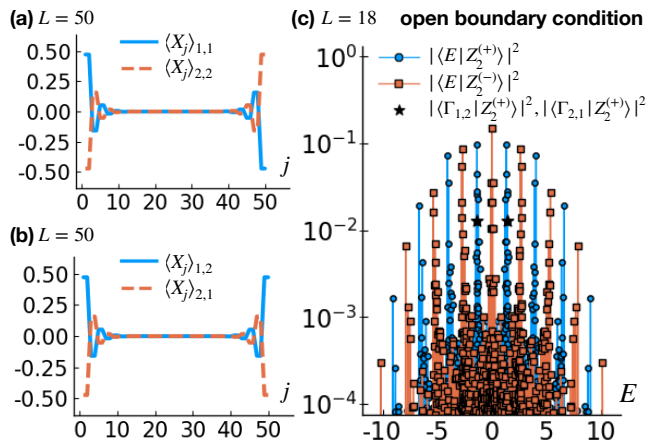
FIG. 1. (a)(b) Energy density profiles $\langle X_j \rangle_{\alpha,\beta}$ in the four exact eigenstates $|\Gamma_{\alpha,\beta}\rangle$ in the OBC system of size $L = 50$. (c)Towers of the Z_2 scar states for OBC found in ED. The positions of the exact scar states $|\Gamma_{1,2}\rangle$ and $|\Gamma_{2,1}\rangle$ are marked with stars.
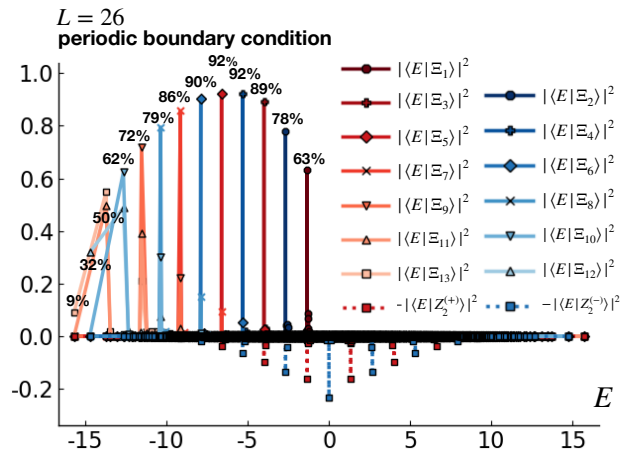
FIG. 2. Overlaps of the SMA and MMA wavefunctions with the eigenstates in the PBC system with $L = 26$. We also list the overlaps with the primary Z_2 scar states. The Z_2 scar states are identified through the overlaps with the $|Z_2^{(+)}\rangle$ or $|Z_2^{(-)}\rangle$ states (for more clarity, we show negatives of these overlaps).

in exact diagonalization (ED). As expected, these $E = \pm\sqrt{2}$ scar states are related by $\mathcal{C}_{\mathrm{ph}}$. Since they are non-degenerate, their finite bond dimension are not related to the exponential degeneracy of the $E = 0$ sector. Their existence again demonstrates the violation of ETH, even without worrying about potential subtleties in the degenerate space [29].

We can also calculate entanglement in $|\Gamma_{\alpha,\beta}\rangle$ for any cut and system size [18, 31]. In the thermodynamic limit, across a cut between C_{2b} and B_{2b+1} (bond-dimension $D = 2$ cut), we find [30] the squared Schmidt values $1/2, 1/2$, which gives the von Neumann entanglement entropy $S_{\mathrm{vN}}^{\mathrm{OBC},D=2} = \ln 2$. Cutting instead across B_{2b+1} and C_{2b+2} ($D = 3$), the squared Schmidt values are $2/3, 1/6, 1/6$, and $S_{\mathrm{vN}}^{\mathrm{OBC},D=3} = -\frac{2}{3}\ln(\frac{2}{3}) - \frac{1}{3}\ln(\frac{1}{6}) \approx 0.868$.

For the states $|\Phi_i\rangle$ in PBC and a large subregion, there are two entanglement cuts, and the entanglement entropy will be the sum of the OBC entropies associated with each cut (and will remain finite in the thermodynamic limit). We can then predict that for the states $|\Phi_{K=0/\pi}\rangle$, the entanglement entropy will be $S_{\mathrm{vN}}^{\mathrm{PBC}} = S_{\mathrm{vN}}^{\mathrm{OBC},D=2} + S_{\mathrm{vN}}^{\mathrm{OBC},D=3} + \ln 2 \approx 2.254$.

Possible relation to Z_2 scar states.- Turner *et. al.* [13, 14] focused on the PXP model with PBC and identified a set of quantum many-body scar states (called Z_2 scar states) through the overlap of eigenstates $|E\rangle$ with the CDW states $|Z_2\rangle = |10 \dots 10\rangle$ or $|Z_2'\rangle = |01 \dots 01\rangle$. The most prominent such scar states have the largest overlap and the smallest entanglement entropy compared to nearby states, but there are also "bands" (or "towers") of weaker scar states close to each primary one. The con-

secutive primary scar states have an almost equal energy separation of ≈ 1.33. The scar states and this frequency were proposed to be responsible for the strong oscillations observed in quenches from the $|Z_2\rangle$ state.

It is convenient to consider states $|Z_2^{(\pm)}\rangle = (|Z_2\rangle \pm |Z_2'\rangle)/\sqrt{2}$, which have inversion quantum numbers $I = 1$ and $I = -1$ and carry momenta $K = 0$ and $K = \pi$ respectively if in PBC. For L_b even, the Z_2 scar states at energy $E \approx 0$ are found to have $I = 1$ (and $K = 0$ in PBC), while for L_b odd they have $I = -1$ (and $K = \pi$). For a fixed L_b, I (and K in PBC) alternate between these values when going from one primary scar state to the next (and are the same within the band of weaker scar states associated with each primary state). This is illustrated in Figs. 1(c) and 2.

Turner *et. al.* [13, 14] proposed to approximate the primary scar states using "forward scattering approximation" (FSA) starting from the Z_2 state. We propose an alternative picture starting from our exact $E = 0$ states.

First, we note that our exact $E = 0$ scar states are in fact representative of the nearby scar states. For instance, at $L = 26$, the nearby $E \approx \pm 1.34$ scar states have average Rydberg excitation number $\langle E|n_j|E\rangle \approx 0.3476$ while $\langle \Phi_{K=\pi}|n_j|\Phi_{K=\pi}\rangle \approx 0.3355$. Second, we note that for OBC, the exact scar states $|\Gamma_{1,2}\rangle$ and $|\Gamma_{2,1}\rangle$, while not being the primary Z_2 scar states, belong to the first non-zero-energy towers of scar states, as shown in Fig. 1(c). Furthermore, we can understand these exact $E = \pm\sqrt{2}$ scar states as "edge excitations" on top of the $E = 0$ states $|\Gamma_{\alpha,\alpha}\rangle$ (see [30]). We therefore conjecture that for the PBC system as well, the nearby scar states can be un-

derstood as quasiparticle excitations on top of the "vacuum" $|\Phi_i\rangle$.

Motivated by these observations, we construct variational wavefunctions using SMA [32, 33] and generalize it to MMA on top of our exact $|\Phi_i\rangle$ states and aimed to capture the nearby scar states. We start with the following SMA wavefunction $|\Xi_1\rangle = (|M_1\rangle - (-1)^{L_b} T_x |M_1\rangle)/\xi_1$, where

$$|M_1\rangle = \sum_{b=1}^{L_b} \mathrm{Tr}[B^{\sigma_1} C^{\sigma_2} \ldots M^{\sigma_{2b-1} \sigma_{2b}} \ldots B^{\sigma_{L-1}} C^{\sigma_L}]|\sigma_1 \ldots \sigma_L\rangle, \quad (8)$$

and ξ_1 provides normalization $\langle \Xi_1 | \Xi_1 \rangle = 1$. The matrices

$$M^{00} = \begin{pmatrix} 1 & 0 \\ 0 & 1 \end{pmatrix} , \; M^{01} = \begin{pmatrix} \mu_1 & 0 \\ \mu_2 & 0 \end{pmatrix} , \; M^{10} = \begin{pmatrix} 0 & 0 \\ -\mu_2 & \mu_1 \end{pmatrix}$$

are chosen such that the wavefunction satisfies the Rydberg-blockaded constraint and $I|M_1\rangle = (-1)^{L_b-1}|M_1\rangle$, hence $I|\Xi_1\rangle = (-1)^{L_b-1}|\Xi_1\rangle$ (see Ref. [30]). We have also chosen the translation quantum number of $|\Xi_1\rangle$ to be $(-1)^{L_b-1}$, which matches the symmetry sector of the first $E \neq 0$ scar state overlapping with the Z_2 CDW. To make $|\Xi_1\rangle$ as close to an eigenstate as possible, we minimize the energy variance $\sigma_H^2(\mu_1, \mu_2) = \langle \Xi_1 | H^2 | \Xi_1 \rangle - \langle \Xi_1 | H | \Xi_1 \rangle^2$ at fixed L. At $L = 26$, we find optimal parameters $\mu_1 = -1.0876$ and $\mu_2 = -0.6344$, which give $\sigma_H^2 = 0.0263$ and the average energy $\langle \Xi_1 | H | \Xi_1 \rangle = -1.3147$. Remarkably, the optimized state has over 63% overlap with the primary Z_2 scar state at $E \approx -1.3386$ found in ED, as shown in Fig. 2. It is easy to check that $\mu_1' = -\mu_1, \mu_2' = \mu_2$ gives $|\Xi_1'\rangle = (-1)^{L_b-1} \mathcal{C}_{\mathrm{ph}} |\Xi_1\rangle$, which captures the scar state with $E \approx 1.3386$.

To capture other primary scar states and support our picture of quasiparticle excitations, we examine the following MMA wavefunctions $|\Xi_n\rangle = (|M_n\rangle + (-1)^{L_b+n} T_x |M_n\rangle)/\xi_n$, where

$$|M_n\rangle = \sum_{b_1, \ldots, b_n=1}^{L_b}{}' \mathrm{Tr}[B^{\sigma_1} C^{\sigma_2} \ldots M^{\sigma_{2b_1-1} \sigma_{2b_1}} \ldots$$
$$\ldots M^{\sigma_{2b_n-1} \sigma_{2b_n}} \ldots B^{\sigma_{L-1}} C^{\sigma_L}]|\sigma_1 \ldots \sigma_L\rangle , \quad (9)$$

and the summation is constrained to have all b_i distinct and ξ_n is the normalization factor. Such an $|M_n\rangle$ describes some n-particle scattering state and is the most primitive construction where we simply try hard-core exclusion of the particles. For simplicity, we will take M from the optimization of $|\Xi_1\rangle$. Moreover, $|\Xi_n\rangle$ has quantum numbers $T_x = (-1)^{L_b+n}$ and $I = (-1)^{L_b+n}$, matching the symmetry structure of the Z_2 scar states. Unexpectedly, Fig. 2 shows that the overlaps of such simplest MMA wavefunctions and the primary scar states become better with more quasiparticles, up to about $n \approx L_b/2$, while for larger n the overlaps start to decrease. The poorer performance for $n > L_b/2$ is not

surprising: For example, for $n = L_b$, the state $|M_{L_b}\rangle = \bigotimes_{b=1}^{L_b} |0\rangle_{2b-1}(|0\rangle + \mu_1|1\rangle)_{2b} + \bigotimes_{b=1}^{L_b}(|0\rangle + \mu_1|1\rangle)_{2b-1}|0\rangle_{2b} - \bigotimes_{b=1}^{L_b} |0\rangle|0\rangle$, therefore $|\Xi_{L_b}\rangle \sim |M_{L_b}\rangle$ but has spontaneous T_x symmetry breaking and is only a crude approximation to the true nondegenerate fully symmetric ground state. Our MMA states with n close to L_b are similarly expected to be only crude approximations to the actual primary scar states and are seen to be spread over several nearby scar states. On the other hand, the performance of the states with $n < L_b/2$ is truly remarkable. Typically, when adding more quasiparticles without further optimizations, such MMA states become worse with the number of particles added, while our MMA have better overlaps with the primary scar states. Furthermore, our MMA states perform better than the FSA states for $2 \leq n \simeq L_b/2$. For reference, at $L = 26$, the FSA states have overlap 69% with the scar states $E \approx \pm 1.33$ and $68\% - 72\%$, overlaps on the consecutive primary scar states respectively [30]. This suggests that our exact eigenstates at $E = 0$ provide better starting point for understanding the scar states in the PXP model.

Let us further discuss these results. $|\Xi_1\rangle$ and $|\Xi_1'\rangle \sim \mathcal{C}_{\mathrm{ph}}|\Xi_1\rangle$ can be viewed as representing "elementary quasiparticles" with energies $\epsilon_- \approx -1.31$ and $\epsilon_+ = -\epsilon_-$; these particles also carry inversion quantum number -1. It is then natural to expect strong oscillations with frequency ϵ_+ in observables that flip the inversion quantum number. (Observables in experiment and numerics that do not flip I will show frequency $2\epsilon_+$.) Indeed, even though the overlaps of the Z_2 initial state with the primary scar states decrease exponentially with system size, the "quasiparticle creation operators" can also act on many more states, always "adding" roughly $\epsilon_\pm$. This argument resembles the quasiparticle explanation [9] of strong oscillations in the "weak thermalization" regime in Ref. [7], where the initial state happened to be near the ground state. The differences here are that the initial Z_2 state is at $T = \infty$ but is "close" to our special eigenstates $|\Phi_i\rangle$, and that the quasiparticles here can carry both positive and negative energies.

By repeated application of the SMA construction that gave us the $|\Xi_1\rangle$ and $|\Xi_1'\rangle$ states, we also expect additional states with energies $E \approx (n_+ - n_-)\epsilon_+$, $n_+, n_- \in \mathbb{N}$. We have demonstrated the $(n_+, n_-) = (0, n)$ branch explicitly in Fig. 2. Interestingly, the same energy $m\epsilon_+$ can be obtained in multiple ways, which may explain the bands of weaker scar states near the primary states.

Finally, we note that the presented simple "bond-dimension-2" SMA wavefunctions cover cases where we replace one B or one C with an "excitation," or "excite" two consecutive B_{2b-1}, C_{2b} matrices. One can also consider exciting two consecutive C_{2b}, B_{2b+1} matrices, which would lead to new "bond-dimension-3" SMA wavefunctions with more variational parameters and the corresponding MMA wavefunctions. Our study shows that

they can capture the primary Z_2 scar states with even higher fidelity [30], but since the improvement is only quantitative, we presented the simpler bond-dimension-2 SMA.

Conclusions.- We discovered exact scar states in the Rydberg-blockaded atom chain at $T = \infty$ that explicitly violate the strong-ETH and have constant entanglement scaling in subsystem size. Our exact states show translation symmetry breaking, which implies two-fold degeneracy for PBC. The exact scar states for OBC have the same bulk as for PBC and can have different edge terminations leading to different eigenenergies, including nondegenerate energies.

By constructing quasiparticles on top of the exact scar states, we capture the primary Z_2 scar states with high fidelity. Systematic improvements for capturing the primary scar states, as well as study bands of weaker scar states are therefore warranted. For example, even for the SMA, is there a convergent construction that reproduces the first primary Z_2 scar state and proves its ETH-violating properties? It is also interesting to understand the pattern of scar states in the PXP model more generally and how it compares with other instances of exact scar states [17, 18, 20]. Studying additional models with exact scar states and their stability to perturbations would be beneficial for both of these questions. We leave such explorations for future work.

[1] J. M. Deutsch, Phys. Rev. A **43**, 2046 (1991).
[2] M. Srednicki, Phys. Rev. E **50**, 888 (1994).
[3] M. Rigol, V. Dunjko, V. Yurovsky, and M. Olshanii, Phys. Rev. Lett. **98**, 050405 (2007).
[4] M. Rigol, V. Dunjko, and M. Olshanii, Nature **452**, 854 (2008).
[5] H. Kim, T. N. Ikeda, and D. A. Huse, Phys. Rev. E **90**, 052105 (2014).
[6] J. R. Garrison and T. Grover, Phys. Rev. X **8**, 021026 (2018).
[7] M. C. Bañuls, J. I. Cirac, and M. B. Hastings, Phys. Rev. Lett. **106**, 050405 (2011).
[8] M. Kormos, M. Collura, G. Takács, and P. Calabrese, Nat. Phys. **13**, 246 (2016).
[9] C.-J. Lin and O. I. Motrunich, Phys. Rev. A **95**, 023621 (2017).
[10] A. J. A. James, R. M. Konik, and N. J. Robinson, arXiv:1804.09990 (2018), arXiv:1804.09990.
[11] N. J. Robinson, A. J. A. James, and R. M. Konik, arXiv:1808.10782 (2018), arXiv:1808.10782.
[12] H. Bernien, S. Schwartz, A. Keesling, H. Levine, A. Omran, H. Pichler, S. Choi, A. S. Zibrov, M. Endres, M. Greiner, V. Vuletić, and M. D. Lukin, Nature **551**, 579 (2017).
[13] C. J. Turner, A. A. Michailidis, D. A. Abanin, M. Serbyn, and Z. Papić, Nat. Phys. **14**, 745 (2018).
[14] C. J. Turner, A. A. Michailidis, D. A. Abanin, M. Serbyn, and Z. Papić, arXiv:1806.10933 (2018), arXiv:1806.10933.
[15] E. J. Heller, Phys Rev Lett **53**, 1515 (1984).
[16] I. Affleck, T. Kennedy, E. H. Lieb, and H. Tasaki, Phys. Rev. Lett. **59**, 799 (1987).
[17] S. Moudgalya, S. Rachel, B. A. Bernevig, and N. Regnault, arXiv:1708.05021 (2017), arXiv:1708.05021.
[18] S. Moudgalya, N. Regnault, and B. A. Bernevig, arXiv:1806.09624 (2018), arXiv:1806.09624.
[19] O. Vafek, N. Regnault, and B. A. Bernevig, SciPost Phys **3**, 043 (2017).
[20] N. Shiraishi and T. Mori, Phys. Rev. Lett. **119**, 030601 (2017).
[21] T. Mori and N. Shiraishi, Phys. Rev. E **96**, 022153 (2017).
[22] W. W. Ho, S. Choi, H. Pichler, and M. D. Lukin, arXiv:1807.01815 (2018), arXiv:1807.01815.
[23] V. Khemani, C. R. Laumann, and A. Chandran, arXiv:1807.02108 (2018), arXiv:1807.02108.
[24] A. Chandran, M. D. Schulz, and F. J. Burnell, Phys. Rev. B **94**, 235122 (2016).
[25] S. Sachdev, K. Sengupta, and S. M. Girvin, Phys. Rev. B **66**, 075128 (2002).
[26] P. Fendley, K. Sengupta, and S. Sachdev, Phys. Rev. B **69**, 075106 (2004).
[27] I. Lesanovsky, Phys. Rev. Lett. **106**, 025301 (2011).
[28] I. Lesanovsky, Phys. Rev. Lett. **108**, 105301 (2012).
[29] M. Schecter and T. Iadecola, Phys. Rev. B **98**, 035139 (2018).
[30] See Supplemental Material.
[31] J. I. Cirac, D. Poilblanc, N. Schuch, and F. Verstraete, Phys. Rev. B **83**, 245134 (2011).
[32] J. Haegeman, B. Pirvu, D. J. Weir, J. I. Cirac, T. J. Osborne, H. Verschelde, and F. Verstraete, Phys. Rev. B **85**, 100408 (2012).
[33] J. Haegeman, S. Michalakis, B. Nachtergaele, T. J. Osborne, N. Schuch, and F. Verstraete, Phys. Rev. Lett. **111**, 080401 (2013).